A practical acoustic full waveform inversion workflow applied to a 3D land dynamite survey

Jiawei Mei, Qianqian Tong, CGG*

Summary

Full waveform inversion (FWI) has been used to successfully build high-resolution earth velocity models for marine data. For land data sets, FWI using acoustic wave equation (acoustic-FWI) remains challenging due to the lack of modeling of strong surface waves, converted waves, phase dispersion, and near-surface weathering layer distortion. In addition, for land dynamite surveys, the source wavelet information is usually missing, and the recorded individual waveform varies greatly because of the spatially variant shot characteristics such as source charge size, shot depth, and hole-pattern as well as the distortion caused by the near-surface weathering layer. We designed and implemented a practical and comprehensive workflow to mitigate missing source wavelet information and vast spatial variation in the waveforms and to address the common challenges of acoustic-FWI application on land surveys during field data preparation.

Introduction

Compared to traditional ray-based tomography using only kinematic information, FWI uses full waveform information to build high-fidelity and high-resolution models by minimizing the difference between predicted and observed data sets.

Acoustic-FWI has been successfully applied to a wide variety of offshore surveys (Sirgue et al., 2009; Ratcliffe et al., 2013; Mothi et al., 2013); however, it remains challenging for land data for several reasons. Two of these reasons are (1) the field data can be limited by a low signal-to-noise ratio or missing low frequencies and far offsets, and (2) acoustic-FWI is not suitable for strong surface waves, converted waves, phase dispersion, and near-surface weathering layer distortions. In addition, for land dynamite surveys, information on the source wavelet is usually missing. The recorded individual waveform varies greatly because of distortion caused by the near-surface weathering layer as well as spatially variant shot characteristics such as source charge size, shot depth, and hole-pattern. We present a practical and comprehensive workflow to address the common challenges of acoustic-FWI application on land surveys while going one step further to mitigate missing source wavelet information and waveforms with vast spatial variation.

Study area

Our study area, located in southeast Texas, was acquired by a 3D dynamite survey covering approximately 130 sq. miles with small elevation variations from 40 ft to 100 ft. The source interval was 245 ft, and the source line interval was 1540 ft. The receiver patch contained 12 receiver lines with a spacing of 1100 ft, and there were 168 live channels along each cable with a receiver interval of 220 ft. The maximum offset was approximately 27000 ft, while the maximum diving wave penetration depth was approximately 12000 ft for the initial vertical transverse isotropy (VTI) models, which were the smoothed final results of the depth model building after a series of refraction and reflection tomography. Because of the absence of low-frequency energy, time domain acoustic-FWI with data selection (Bi et al., 2014) for a velocity-only update (based on Warner et al., 2013) was performed from 7 Hz to 10 Hz with increments of 1 Hz and eight iterations at each frequency.

Method

Our workflow can be divided into two major steps: (1) estimating the source wavelet and addressing the spatially-variant individual waveform and (2) compensating for the acoustic-FWI limitations.

Source wavelet and spatially-variant waveform

Applying FWI requires the source function. For onshore vibroseis surveys, the source wavelet can be estimated based on vibrator sweep information. For dynamite surveys, there are two common approaches for source wavelet estimation: (1) using a common offset stack of the first arrival or (2) solving a linear inverse problem relating the misfit to the source function (Pratt, 1999). However, the first approach may mix shot characteristics and near-surface distortion, while the second approach is based on spectral matching, which is not accurate for acoustic modeling, as well as the assumption that the velocity model is close to the true one, which is generally not the case.

In our workflow, the source wavelet is estimated from the surface-consistent deconvolution (Taner et al., 1981; Garceran et al., 2012; Zhang et al., 2015). In surface-consistent deconvolution, the recorded seismogram can be modeled as:

$$x_{ij}(t) = w(t) * s_i(t) * e_k(t) * h_l(t) * r_j(t) \cdots + n(t), \quad (1)$$

where $x_{ij}(t)$ is the recorded seismogram, $w(t)$ is the average source waveform, and $s_i(t)$ is the convolution of the effects the near-surface imposes on the down-going source wavefront at surface position i and the deviation of source

DOI http://dx.doi.org/10.1190/segam2015-5850377.1

waveform at position i from the average source waveform. Similarly, $r_j(t)$ is the influence of the near-surface on the up-going wavefront at receiver location j (receiver deviation is very small because receivers are usually well calibrated), $e_k(t)$ is the earth reflectivity, $h_l(t)$ is the offset dependent term where $l=j-i$, $n(t)$ is random noise, and $*$ represents convolution. The average shot waveform $w(t)$ is used as the source wavelet. The corresponding deconvolution operators of $s_i(t)$ and $r_j(t)$ are applied on the input field data to FWI to address the spatial varying source waveform due to the varying source characteristics as well as the distortion caused by the near-surface weathering layer, which acoustic-FWI cannot accommodate.

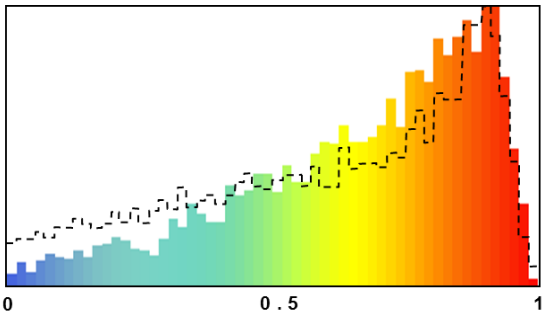

Figure 1: Histogram of zero-lag cross-correlation values of one cross-spread between field data and full waveform inversion (FWI) synthetics. The black dashed line represents the FWI input field data with no deconvolution, while the color histogram represents surface consistent two-term deconvolution applied to the field data prior to FWI work. The color histogram shows better similarity.

Figure 1 shows the zero-lag cross-correlation of one cross-spread between field data and synthetics based on FWI models up to 10 Hz. The similarity between the field data and the corresponding synthetic data is improved when two-term deconvolution (Zhang et al., 2015) is applied to the input field data prior to FWI.

Acoustic-FWI compensation

Because surface and shear wave propagations are not modeled by the acoustic wave equation, they are attenuated using adaptive ground roll attenuation (Le Meur et al., 2008) during field data preparation to compensate for the acoustic-FWI non-elastic limitation. In addition, because sedimentary rocks are not purely elastic media, wavefield energy is partially converted to heat during propagation. This dissipative effect introduces both amplitude attenuation and phase dispersion. The dependence of phase velocity on frequency (Futterman, 1962; Robinson, 1979; Kjartansson, 1979) for a relatively large, constant quality factor Q is given by:

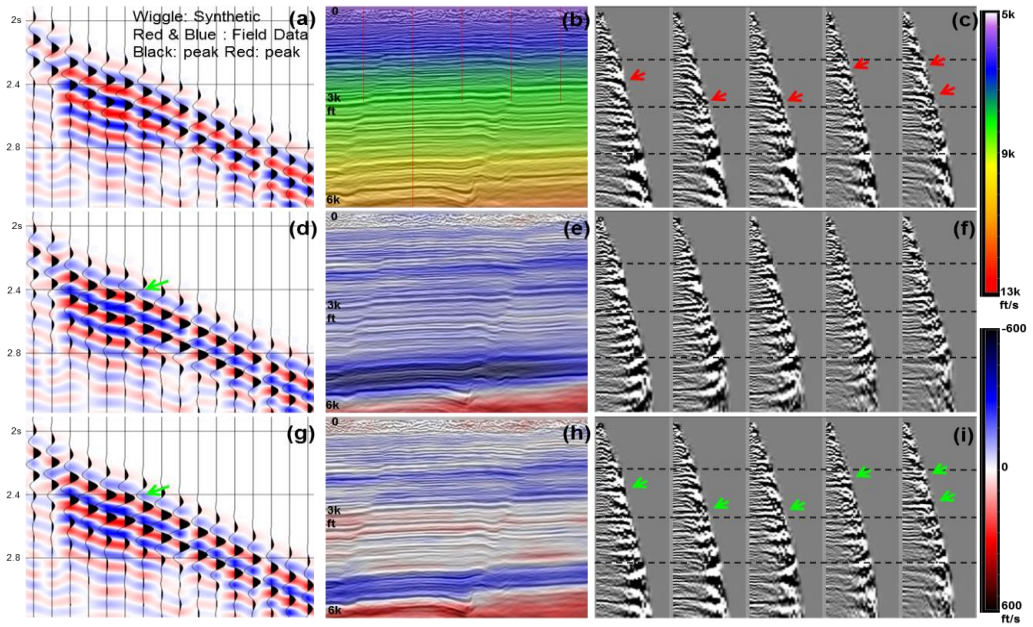

Figure 2: Phase Q effect QC. Initial model: (a) synthetic data, (b) overlaid on the migration section, and (c) common image gathers (CIGs). FWI-updated model with no phase Q correction on the FWI input data: (d) synthetic data, (e) perturbation of model overlaid on the corresponding migration section, and (f) CIGs. FWI-updated model with phase Q correction on the FWI input data: (g) synthetic data, (h) perturbation of model overlaid on the corresponding migration section, and (i) CIGs. Green arrows in (d) and (g) indicate the time shift on the FWI input due to phase Q correction. Red lines indicate the CIG QC locations. Arrows in (c) and (i) indicate where the CIG flatness improved. (Seismic data is owned or controlled by Seismic Exchange, Inc.; interpretation is that of CGG.)

DOI http://dx.doi.org/10.1190/segam2015-5850377.1

$$\frac{V_r}{V} \cong 1 - \frac{1}{\pi Q} \ln\left(\frac{\omega}{\omega_r}\right), \qquad (2)$$

where ω_r is the reference angular frequency, and V_r is the propagation velocity at the reference frequency. Due to phase dispersion, the low-frequency energy propagates slower than the high-frequency energy. FWI primarily uses low-frequency field data to obtain a high-resolution earth model, which is too slow for the image domain QC because the migration input usually has a much higher dominant frequency and/or phase Q correction applied to it. After four iterations at 7 Hz, the synthetic data of the FWI-updated model without phase Q correction on the input (Figure 2d) matched the field data better than the initial model (Figure 2a), but the flatness QC of the common image gathers (CIGs) shows that the FWI-updated model was too slow for migration input (Figure 2f), which has a dominant frequency around 20 Hz and phase Q correction. The FWI-updated model from the input field data with phase Q correction not only matched the field data in the data domain (Figure 2g), but it also improved the CIG flatness in the image domain (Figure 2i). Therefore, phase dispersion needs to be addressed for acoustic-FWI non-visco limitation. To address the primary frequency discrepancy between the FWI input and the migration input, a constant phase Q140 correction was applied on both the inputs.

Application and results

Consistent data preparation was applied to both the FWI input and the migration input. The FWI-updated model was validated using a synthetic QC in the data domain and a migration QC in the image domain using controlled beam migration (CBM) (Vinje et al., 2008). The data domain QC showed that the synthetic data with the updated model matched the field data better than the initial model (Figure 3).

Compared to the initial model (Figure 4a), the FWI output (Figure 4b) had a higher resolution and conformed to the geology better. The outline of channels in the model matched the image very well (Figure 4d). The migration depth slice of the updated model showed improved focusing of the channels and clearer fault positions.

Figure 5 shows the very shallow migrated images before and after the FWI update. After the update, the event continuity was improved, and the shallow structures were more geologically plausible. Figure 6 shows the migration section up to 12000 ft deep. The event focusing was improved and some missing events appeared with the FWI-updated model. The overall CIG flatness was improved as well.

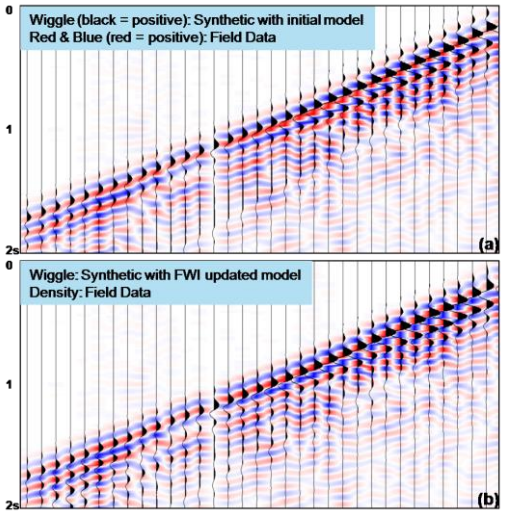

Figure 3: Synthetic QC: synthetic data of the (a) initial model and (b) FWI-updated model. (Seismic data is owned or controlled by Seismic Exchange, Inc.; interpretation is that of CGG.)

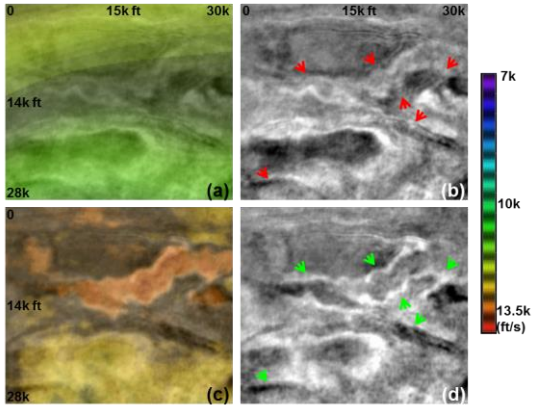

Figure 4: (a) Initial velocity model overlaid on the seismic depth slice. (b) Controlled beam migration (CBM) depth slice of initial model. (c) FWI-updated velocity model overlaid on the seismic depth slice. (d) CBM depth slice of FWI-updated model. The FWI-updated model confromed to the geology well. Arrows in (b) and (d) indicate the improved focusing of channels and clearer fault positions. (Seismic data is owned or controlled by Seismic Exchange, Inc.; interpretation is that of CGG.)

Conclusion

By applying this workflow to an acoustic-FWI application of a southeast Texas data set, we obtained an uplift of the image based on the FWI-derived velocity model. The details predicted in the FWI model conformed to the geology well. The CIG flatness and the event continuity and focusing were improved overall. This workflow is suitable for vibroseis surveys as well. There are two major

DOI http://dx.doi.org/10.1190/segam2015-5850377.1

approximations in this workflow: constant Q for phase dispersion correction and surface-consistent deconvolution with minimum phase assumption. A space and time variant Q and surface-consistent phase correction without minimum phase assumption can be integrated into the workflow to further improve the result. In this case study, we found that consistent data preparation is critical to validating the FWI update in the image domain. With consistent inputs, the residual CIG curvature could be due to the anisotropy errors.

Acknowledgements

The authors thank CGG and BP for permission to publish this work. Acknowledgements also go to Seismic Exchange, Inc. for permission to show the seismic data. We thank Jingfeng Zhang and Walt Fulroth from BP and Tony Huang, Chu-Ong Ting, Tao Lin, and Adam Searle from CGG for continuous input and feedback during the course of this work. We also thank Shoaib Ahmed for data preparation and the CGG FWI programming team for valuable insight and support.

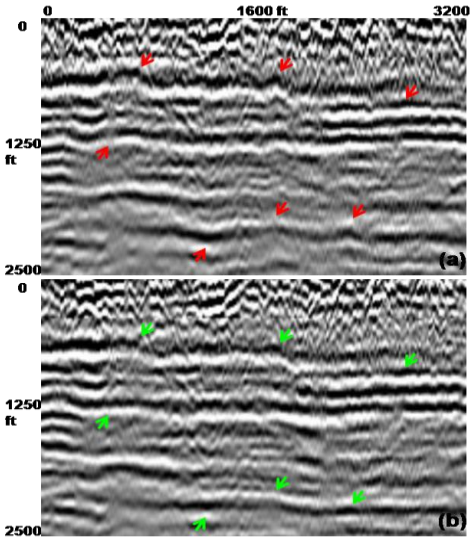

Figure 5: (a) Shallow migrated section using initial model. (b) Shallow migrated section using FWI-updated model. The shallow event continuity was improved, and the shallow structures were more geologically plausible. (Seismic data is owned or controlled by Seismic Exchange, Inc.; interpretation is that of CGG.)

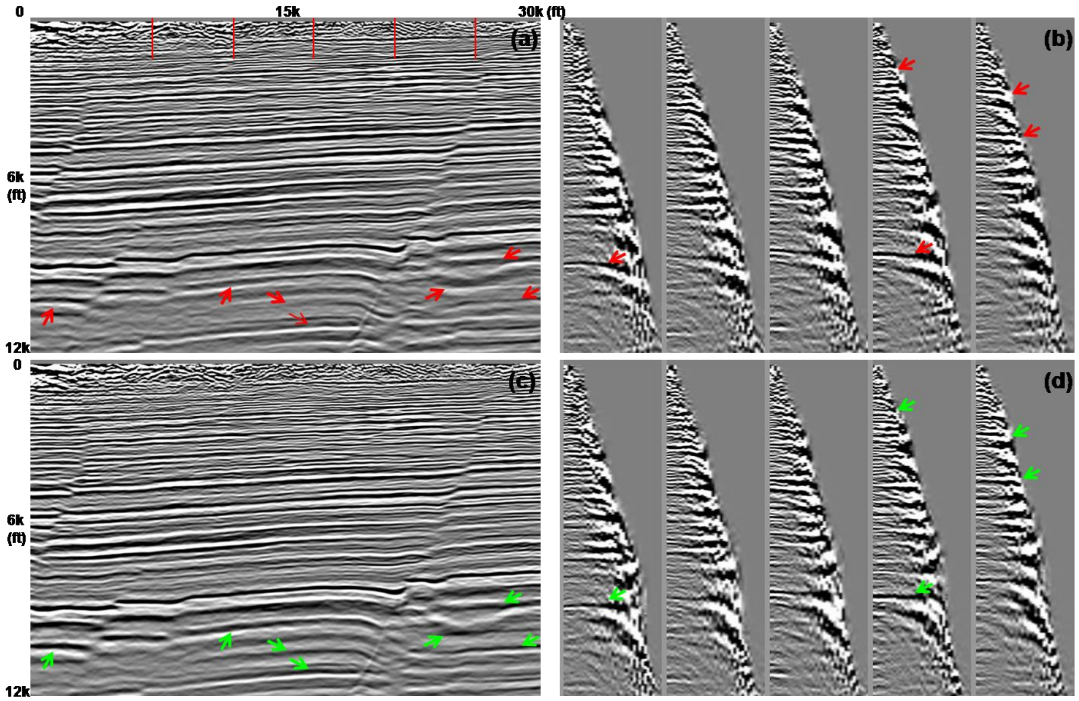

Figure 6: (a) Migration section with initial model. (b) CIG with initial model. (c) Migration section with FWI-updated model. (e) CIG with FWI-updated model. Red lines indicate the CIG QC locations. The event focusing and the overall CIG flatness were improved. (Seismic data is owned or controlled by Seismic Exchange, Inc.; interpretation is that of CGG.)

DOI http://dx.doi.org/10.1190/segam2015-5850377.1

EDITED REFERENCES

Note: This reference list is a copyedited version of the reference list submitted by the author. Reference lists for the 2015 SEG Technical Program Expanded Abstracts have been copyedited so that references provided with the online metadata for each paper will achieve a high degree of linking to cited sources that appear on the Web.

REFERENCES

Bi, H., and T. Lin, 2014, Impact of adaptive data selection on full waveform inversion: 84th Annual International Meeting, SEG, Expanded Abstracts, 1094–1098.

Futterman, W. I., 1962, Dispersive body waves: Journal of Geophysical Research, **67**, no. 13, 5279–5291, http://dx.doi.org/10.1029/JZ067i013p05279.

Garceran, K., and D. Le Meur, 2012, Simultaneous joint inversion for surface-consistent amplitude and deconvolution: 74th Conference and Exhibition, EAGE, Extended Abstracts, C015, doi:10.3997/2214-4609.20148167.

Kjartansson, E., 1979, Constant *Q*-wave propagation and attenuation: Journal of Geophysical Research Solid Earth, **84**, B9, 4737–4784, http://dx.doi.org/10.1029/JB084iB09p04737.

Le Meur, D., N. Benjamin, R. Cole, and M. Al Harthy, 2008, Adaptive groundroll filtering: 70th Conference & Exhibition, EAGE, Extended Abstracts, doi:10.3997/2214-4609.20147745.

Mothi, S., K. Schwarz, and H. Zhu, 2013, Impact of full-azimuth and long-offset acquisition on full waveform inversion in deep water Gulf of Mexico: 75th Conference & Exhibition, EAGE, Extended Abstracts.

Pratt, R. G., 1999, Seismic waveform inversion in the frequency domain, Part 1: Theory and verification in a physical scale model: Geophysics, **64**, 888–901, http://dx.doi.org/10.1190/1.1444597.

Ratcliffe, A., R. Jupp, R. Wombell, G. Body, V. Durussel, A. Fernandes, B. Gosling, and M. Lombardi, 2013, Full-waveform inversion of variable-depth streamer data: An application to shallow channel modeling in the North Sea: The Leading Edge, **32**, 1110–1115, http://dx.doi.org/10.1190/tle32091110.1.

Robinson, J. C., 1979, A technique for continuous representation of dispersion on seismic data: Geophysics, **44**, 1345–1351, http://dx.doi.org/10.1190/1.1441011.

Sirgue, L., O. I. Barkved, J. P. Van Gestel, O. J. Askim, and J. H. Kommedal, 2009, 3D waveform inversion on Valhall wide-azimuth OBC: 71st Conference & Exhibition, EAGE, Extended Abstracts, U038, doi:10.3997/2214-4609.201400395.

Taner, M. T., and F. Koehler, 1981, Surface consistent corrections: Geophysics, **46**, 17–22, http://dx.doi.org/10.1190/1.1441133.

Vinje, V., G. Roberts, and R. Taylor, 2008, Controlled beam migration: A versatile structural imaging tool: First Break, **26**, no. 9, 109–113.

Warner, M., A. Ratcliffe, T. Nangoo, J. Morgan, A. Umpleby, N. Shah, V. Vinje, I. Štekl, L. Guasch, C. Win, G. Conroy, and A. Bertrand, 2013, Anisotropic 3D full-waveform inversion: Geophysics, **78**, no. 2, R59–R80.

Zhang, J., C. Klemm, S. Michell, A. Gangopadhyay, J. Mei, J. Connor, and S. Ahmed, 2015, Quality control of surface-consistent deconvolution on land dynamite data: The Leading Edge, **34**, 430–436, http://dx.doi.org/10.1190/tle34040430.1.

DOI http://dx.doi.org/10.1190/segam2015-5850377.1